Hydrogen Production *via* Thermal Cracking of Ammonia Using Steel Fiber Catalyst

Bo Zhang,* Mingyue Zhao, Kangwei He, and Jianye Huang

Due to challenges associated with hydrogen storage and transportation, on-site hydrogen production has garnered significant attention. However, achieving a balance between efficiency and cost remains a critical challenge in the catalytic conversion of ammonia to hydrogen. Catalysts utilizing carbon fiber supports derived from cellulose, which contain a high carbon content, have demonstrated promising dehydrogenation activity in ammonia pyrolysis. One such catalyst component is steel fiber which contains a high content of transition metals and serves as a connection between the carbon element and the metals, which would enhance its catalytic properties. In this study, the catalytic performance of commercial steel fiber for hydrogen production *via* ammonia pyrolysis was investigated. Activity tests and analytical characterizations revealed that the steel fiber catalyst exhibited excellent catalytic activity, stability, and cyclic performance, enabling COX-free hydrogen production. Characterization results indicated that the catalyst contained over 80 wt% iron atoms and exhibited low surface area. The Fe atoms were further converted into stable Fe-N bonds, with the number of Fe-N bonds decreasing as the reaction temperature increased, thereby accelerating the desorption rate of nitrogen atoms on the catalyst surface and enhancing conversion efficiency.

DOI: 10.15376/biores.20.2.4416-4431

Keywords: Ammonia; Hydrogen; Catalytic cracking; Steel fiber; Fe-based catalyst

*Contact information: Institute for Energy Research, Jiangsu University, Zhenjiang 212013, People's Republic of China; *Corresponding author: zb1987@ujs.edu.cn*

INTRODUCTION

Reducing the greenhouse gas emissions from the consumption of traditional fossil fuels is critical to mitigating climate change and its impacts. This can be achieved by transitioning to renewable energy sources and improving energy efficiency in the industry and transportation sectors. Hydrogen, as a green energy source, produces zero emissions during consumption and has attracted significant global attention recently (Naseem *et al.* 2020). However, several critical characteristics, such as leakiness, flammability, and combustibility, pose challenges in its storage and transportation (Ji *et al.* 2021; Adamou *et al.* 2023). On-site hydrogen generation from hydrogen carriers appears to be a promising solution to overcome these disadvantages. Ammonia, with over 17 wt% hydrogen content —higher than that of methanol, cyclohexane, and metal hydrides—has recently gained increased interest (Zhai *et al.* 2020; Andriani and Bicer 2023). Ammonia decomposition is a typical endothermic process with an enthalpy change of 91.2 kJ/mol, requiring temperatures above 400 °C for complete conversion theoretically (Lucentini *et al.* 2021). Therefore, high energy input is necessary to break down ammonia molecules, resulting in

a rich stream of hydrogen and nitrogen (Fedorova *et al.* 2023). Direct heating, known as thermal cracking, is a stable and readily available energy supply method.

Catalytic thermal cracking has gained momentum in past decades, as it can efficiently lower the reaction temperature of ammonia decomposition (Su *et al.* 2023). Catalysts, including noble metals, non-noble metals, alloys, and their compounds, have been extensively investigated (Borisov *et al.* 2023; Fang *et al.* 2023; Bao *et al.* 2024). However, due to the varying experimental conditions used in these studies, comparing the performance of different catalyst systems remains challenging. Studies have verified excellent activity of ruthenium-based catalysts in ammonia thermal cracking, particularly at lower temperatures (Kim and Park 2023; Ju *et al.* 2024). Ganley *et al.* (2004) investigated the catalytic activity of different metals supported on Al_2O_3 and established the activity order as Ru > Ni > Rh > Co > Ir > Fe ≫ Pt > Cr > Pd > Cu ≫ Te, Se, Pb. Nevertheless, further research is needed to balance the high cost of noble metal catalysts and their effectiveness (Xie *et al.* 2019). Non-noble metals, due to their abundant availability and acceptable activity, are promising candidates for large-scale industrial production of hydrogen. The decomposition of ammonia using various non-noble metals is currently under extensive study (Al-Shafei *et al.* 2023; Chen *et al.* 2023; He *et al.* 2023). Some non-noble catalysts, such as Ni, Fe, and Co, exhibit activity comparable to that of noble metals (Lee *et al.* 2023). However, reaction mechanisms vary, depending on the material types and specific reaction conditions. Ganley *et al.* (2004) concluded that nitrogen desorption was rate-limiting step for Fe, Co and Ni catalysts, whereas N–H bond scission is the limiting step for Rh, Ir, Pd, Pt, and Cu. To date, the pathways of the ammonia decomposition for different catalysts have not been conclusively determined.

Among the above non-noble metals, iron (Fe) is the most common metal, having been widely used as a catalyst in industrial processes (Man *et al.* 2021; Ahmed *et al.* 2024). Iron is also the most cost-effective metal, with a relatively low global warming power over a 100-year period (Fig. 1) (Nuss and Eckelman 2014; Lucentini *et al.* 2021).

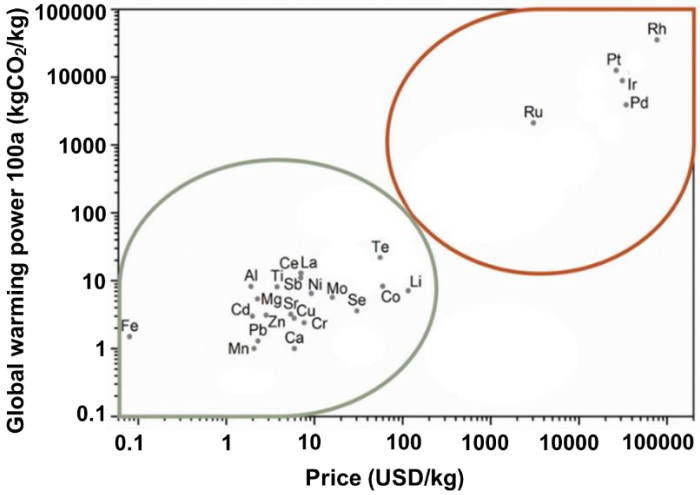

Fig. 1. Comparison of the price and global warming power of the elements

Since the decomposition of ammonia is the inverse reaction of the Haber-Bosch process for the ammonia synthesis, the same Fe catalyst used in ammonia synthesis is also relevant for its inverse process, based on the principle of microscopic reversibility in heterogeneous catalysis (Devkota *et al.* 2024; Skubic *et al.* 2024). Fe nanoparticles

supported on commercial carbon nanotubes (CNTs) have been reported to exhibit good performance in ammonia decomposition under lower Fe loading (Zhang *et al.* 2007). Fe supported on ZSM-5 achieved a high conversion rate of over 99% at 650 ℃ and a space velocity of 30 L/g/h, as reported by Hu *et al.* (2018). Additionally, a Fe-CNFs/mica catalyst achieved over 98% ammonia conversion rate at a lower temperature of approximately 600 ℃, as reported by Duan *et al.* (2011). The study of Fe-based catalysts for ammonia decomposition highlights the structural and support sensitivities of this metal (Bell and Torrente-Murciano 2016).

The support material plays an important role in the catalyst system. Cellulose, a major component of biomass, is one of the most abundant biomaterials worldwide (Ren *et al.* 2023; Ji *et al.* 2023). Carbon fiber derived from cellulose is frequently studied as a support for catalytic processes due to its stability, hydrophobicity, and porosity (Zhang *et al.* 2019). However, most studies have used impregnation or physical incorporation of metal-based catalysts, which may not achieve an ideal connection between the active phase and carbon-based support. Cellulose is a suitable component for combining with metals in special steel production (Ma *et al.* 2024). Steel fiber, an available commercial product, is soft, easily compressed, and stretchable. Steel fiber is a commonly used admixture material for cement in the construction industry and is also a common cleaning and polishing tool. Previous studies have shown that the most abundant elements in steel-based materials were iron (Yu *et al*. 2025). The steel-based materials displayed excellent catalysis and adsorption capacity (Hou *et al.* 2024). Steel fiber can be easily loaded, evenly distributed, and induces negligible pressure drop in the flow, making it good for cracking reactions. To date, steel fiber has rarely been studied in the field of ammonia decomposition. In this study, the steel fiber catalyst, which contains a significant amount of Fe element and carbon atoms with a unique cotton-like structure, was investigated for ammonia thermal cracking. The activity of the fiber catalyst for hydrogen production from ammonia was explored, and the catalytic mechanism was discussed, providing a basis for the subsequent catalyst design.

EXPERIMENTAL

Materials

Commercial steel fiber was purchased from Ezhou Baofeng Metal Mold Technology Co., Ltd. This steel fiber, labeled as 0000#, has an average width of approximately 0.03 mm.

Catalyst Preparation

The steel fiber was initially washed in analytical-grade alcohol (Macklin, >99.5%) to remove any potential organic contaminants, followed by thorough washing in deionized water. After washing, all samples were dried in an oven at 105 ℃ overnight. The catalysts were then sealed for further performance tests and analysis.

Catalyst Characterization

An X-ray diffractometer (XRD 6100, Shimadzu, Japan) equipped with Cu Kα radiation was used for measurement. The 2θ range was recorded from 5º to 90º at a step size of 7º/min. Nitrogen adsorption/desorption measurements were performed using a TriStar II 3020 at 77 K. Prior to measurements, the catalysts were degassed in a vacuum atmosphere at 300 ℃ for 3 h. The specific surface area was determined using the Brunauer-

Emmett-Teller (BET) equation. X-ray photoelectron spectra (XPS) were obtained using an ESCALAB QXi spectrometer (Thermo Scientific, USA) with Al Kα radiation. All spectra were corrected using the C 1s signal at a binding energy of 284.8 eV. The morphology of catalysts was analyzed using a field emission scanning electron microscope (MIRA, TESCAN, Czech Republic) at 3 kV under a high vacuum. Elemental mapping was performed simultaneously with morphology analysis, using an energy-dispersive X-ray spectrometer (EDX) at 20 kV. H_2 temperature-programmed reduction (H_2-TPR) analysis was conducted using a chemisorption analyzer (PCA-1200, Beijing Builder Electronic Co. Ltd., China). The samples were heated to 200 ℃ and maintained for 1 h in an N_2 atmosphere. Subsequently, they were cooled to 25 ℃ and heated to 800 ℃ in the flow of 10% H_2/N_2 at 30 mL/min, with a thermal conductivity detector (TCD) located downstream to monitor hydrogen consumption. Temperature-programmed desorption (TPD) experiments were conducted in the same chemisorption analyzer. The samples were heated to 200 ℃ and maintained for 1 h in a He flow. They were then cooled to 25 ℃, and a mixture of 10% ($NH_3/H_2/N_2/CO_2$)/He was injected into the sample at a flow rate of 100 mL/min for 30 min. Finally, the samples were heated to 800 ℃ in a He flow, with the TCD detector monitoring the amount of desorbed gas.

Catalyst Performance

Active test

The catalytic ammonia decomposition characteristics were evaluated with a quartz fixed-bed reactor (inner diameter of 8 mm, external diameter of 24 mm) using a 3-kW furnace for heating. During the experiment, a fixed 500 mg catalyst was loaded in the middle of the reactor and heated to the desired temperature (450 to 700 ℃, at intervals of 50 ℃) at a heating rate of 15 ℃/min. For the activity test, 15 mL/min nitrogen was used as the purge gas during the temperature-raising stage. Once the set temperature was reached, pure ammonia was injected at flow rates ranging from 15 to 60 mL/min. The flow rates of inlet gas were controlled by a mass flow controller (Alicat, accuracy of ± 0.4% reading +0.2% of full scale, control range of 0 to 100 mL/min), and the outlet data were recorded by a mass flow meter (Alicat, accuracy of ± 0.6% of reading, 0 to 200 mL/min). The reaction time was set to 8 h for the activity test and 18 h for the stability test. The ammonia conversion, which doubled the volume of the product gas, was calculated using Eq. 1,

$$NH_3\ \text{Conversion}\ (\%) = F_{outlet}/2F_{inlet} \times 100\% \quad (1)$$

where F_{inlet} is the inlet ammonia flow rate, and F_{outlet} is the outlet gas flow rate in mL/min, measured after unreacted ammonia was absorbed by a sulfuric acid solution.

Kinetic calculation

The apparent reaction rate of ammonia cracking was calculated as follows:

$$r = \frac{V_1 \times X_{NH_3}}{22.4W} \quad (2)$$

where V_1 is the inlet flow rate of ammonia, X_{NH_3} is the ammonia conversion rate, and W is the weight (kg) of the catalyst.

The apparent activation energy (E_a) for ammonia cracking was calculated using Eq. 3 (Zhang, *et al*. 2014),

$$\ln r = -E_a/RT + n \quad (3)$$

where r is calculated from Eq. 2, T is the reaction temperature (K), R is the gas constant (8.314 J/(mol*K)), and E_a is calculated from the slope of the plot of T^{-1} versus ln$r$.

RESULTS

Catalyst Performance

The catalyst activity of the steel fiber for ammonia decomposition was evaluated at different temperatures and reaction times, as shown in Fig. 2. The catalyst was subjected to the decomposition reaction at 450, 550, and 650 ℃ for 18 h, with a total space velocity of 1800 mL/g/h. After the reaction, the catalyst was cooled and maintained under an Ar atmosphere for 24 h under Ar. Subsequently, it was tested again under the same conditions to assess its cyclic stability, and the results are presented in Fig. 2A. It is evident that the steel fiber exhibited good cyclic performance in terms of ammonia conversion across all three conditions.

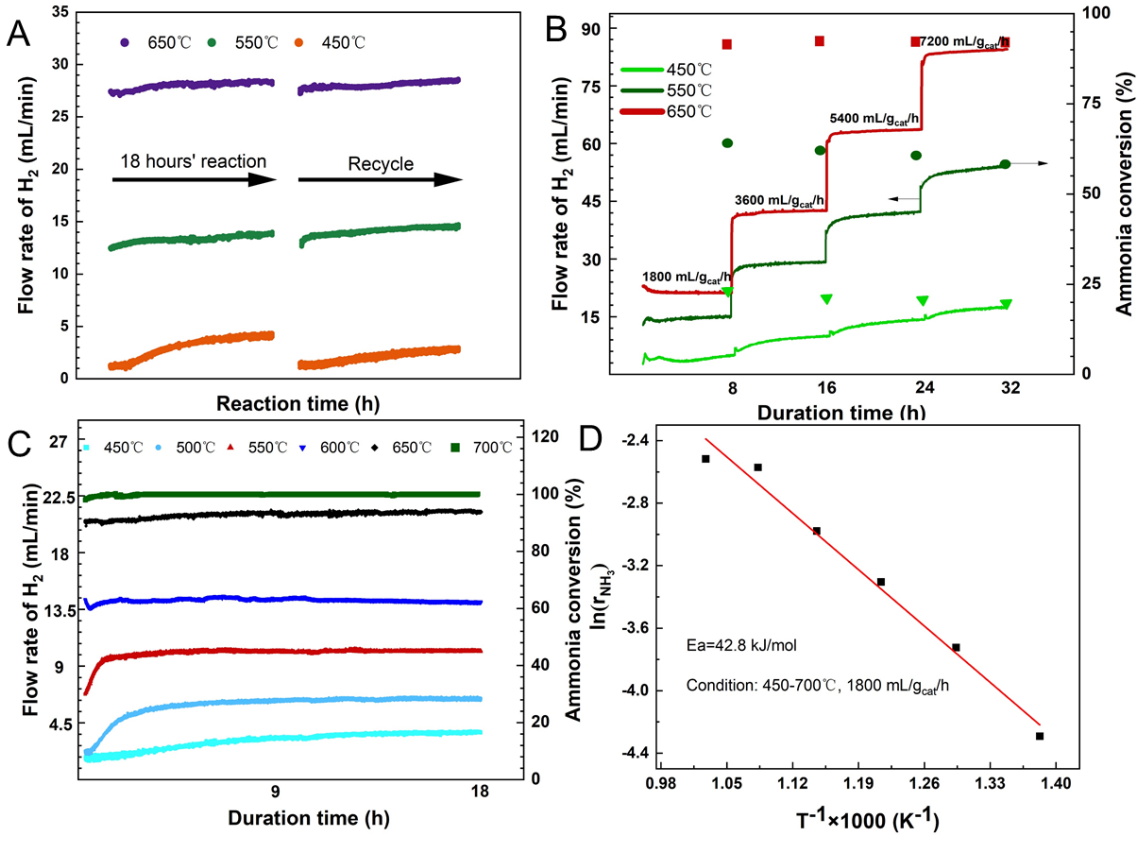

Fig. 2. Catalytic performance of the steel fiber on pure ammonia conversion: (A) Cyclic stability, (B) Effect of space velocity, (C) Catalytic stability, and (D) Kinetic plot

The catalyst activity was further evaluated by varying the total space velocity and reaction temperature, as shown in Fig. 2B. As shown, it is evident that the reaction on the catalyst stabilized within 8 h of reaction time. Since ammonia cracking is an endothermic process, the extent of the reaction is highly dependent on temperature. As illustrated in Fig. 2B, the increase in conversion rate from 550 to 650 ℃ was less pronounced compared to

that from 450 to 550 ℃, suggesting a potential shift in the reaction pathway. Furthermore, the ammonia conversion rate trend in Fig. 2B indicates increasing the total space velocity had minimal impact on the conversion rate at 650 ℃, whereas a noticeable decrease was observed at 450 and 550 ℃. The stability of the steel fiber for ammonia cracking was tested using pure ammonia at temperatures ranging from 450 to 700 ℃ for 18 h, with a total space velocity of 1800 mL/g/h. The results are presented in Fig. 2C. As shown in the figure, the catalyst performance stabilized after approximately 8 h at 450 ℃, with the acquired stabilization time decreasing as the reaction temperature increased. Throughout the 18 h test, all cases showed stable ammonia decomposition. The ammonia rate was around 18% at 450 ℃ and increased with the rising temperature, reaching complete decomposition at 700 ℃. Kinetic calculation and fitting were performed, and results are demonstrated in Fig. 2D. The apparent activation energy was calculated to be 42.8 kJ/mol.

To better understand the performance of Fe-based fiber catalyst for ammonia decomposition, a comparison was made with other Fe-based catalysts in literature, and results are listed in Table 1. All the Fe-based catalysts exhibited good activity in ammonia conversion. The catalyst in this study demonstrated excellent performance even without pre-reduction, achieving conversion rates above the average reported in literature.

Table 1. Comparison of the Catalysts (This Study and Other Publications)

Catalyst	WHSV (mL/g/h)	Temperature (ºC)	Conversion (%)	Reference
Fe	18000	500	30	Xun *et al*. 2017
Fe/CNFs	6500	600	51	Duan *et al*. 2011
Fe/CNTs	6000	500	15	Zhang *et al*. 2013
Fe/Mica	6500	600	85	Duan *et al*. 2011
Fe/GC	6000	600	71	Li *et al*. 2017
Fe (CaO, K_2O)	2000	500	46	Arabczyk *et al*. 1999
Fe-based Fiber	1800	500	29	This work
Fe-based Fiber	1800	600	63	This work

Catalyst Characterizations

To elucidate the role of steel fiber in enhancing ammonia cracking, a series of characterization techniques were employed. The morphology analysis of the catalyst (Fig. 3) at 5000× magnification revealed a fiber-like structure composed of C, Mn, O, and Fe, with Fe being the predominant element, accounting for over 85 wt% of the sample. Nitrogen adsorption/desorption measurements indicated that the steel fiber had a BET surface area of 0.33 m^2/g, confirming its non-porous nature. This characteristic distinguishes it significantly from catalysts reported in previous studies.

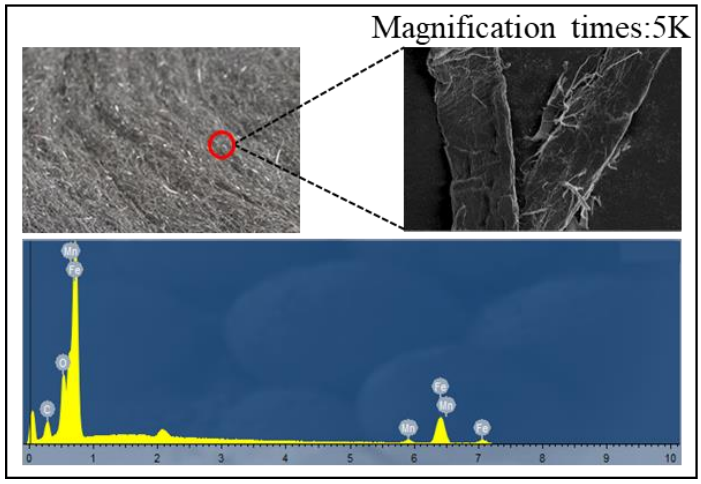

Fig. 3. The structure of the steel fiber

X-ray diffraction analysis of the catalyst

Figure 4 shows the XRD patterns of the fresh and spent catalysts after cracking at 450, 550, and 650 ℃. In the fresh catalyst, diffraction peaks corresponding to FeO (PDF#74-1886) and $Fe_{19}Mn$ (PDF#65-7528) were observed. After ammonia cracking at 450 ℃, the appearance of Fe diffraction peaks (PDF#06-0696) in the spent catalyst indicated the reduction of FeO to metallic Fe by ammonia. The increased peak intensities of metallic Fe and $Fe_{19}Mn$ suggested a relatively high content of these items. When the cracking temperature was increased to 550 ℃, the spent catalyst exhibited prominent diffraction peaks corresponding to Fe_4N (PDF#83-0875). Upon further increasing the reaction temperature to 650 ℃, diffraction peaks of metallic Mn (PDF#89-4253) emerged in the spent catalyst. Additionally, the intensity of the Fe_4N diffraction peak decreased at 650 ℃ compared with that at 550 ℃, suggesting improved dispersion of Fe_4N at higher temperatures.

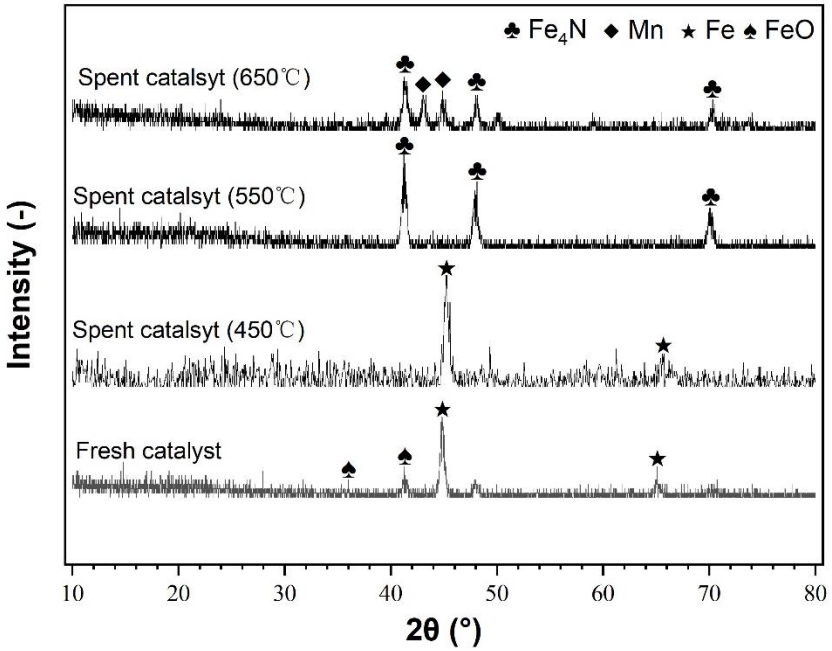

Fig. 4. Powder XRD patterns of the fresh and spent steel fiber catalyst

FTIR analysis of the catalyst

The structural characteristics of fresh and spent catalysts were investigated using Fourier transform infrared spectroscopy (FTIR) with a Nicolet iS-50 spectrometer (Thermo Fisher Scientific, USA). As shown in Fig. 5, the FTIR spectra revealed significant changes in functional group vibrations. The attenuated C-O stretching vibration observed between 1100 and 1700 cm^{-1} suggests possible reduction of the surface oxygen by the on-site hydrogen, leading to H_2O formation. This hypothesis is also supported by the intensified O-H stretching vibration at 3000-3800 cm^{-1}. Notably, the infrared spectra of the spent catalyst displayed stretching vibrations of C-N at around 2300 cm^{-1}, which may be attributed to adsorbed nitrogen on the catalyst surface during the reaction process.

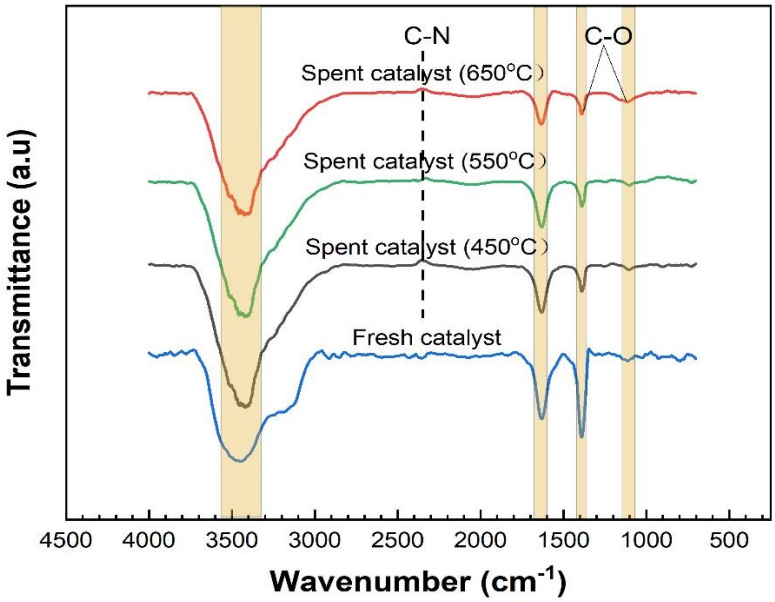

Fig. 5. FTIR patterns of the fresh and spent steel fiber catalyst

Surface morphology of the catalyst

The surface morphology evolution of catalysts before and after reaction was systematically characterized through SEM-EDS. Figures 6A, B, C, and D refer to the fresh catalyst and the spent catalysts of 450, 550, and 650 °C, while numbers of -1, -2, and -3 represent three magnifications from low to high. The fresh catalyst demonstrated a width of 0.028 mm, while the spent catalysts all displayed an expansion after ammonia cracking. The fresh catalyst is a compact material with a nonporous structure, which is in agreement with the BET surface area analysis. Post-reaction samples showed some pores formation in the fiber matrix. This structural modification likely originates from ammonia-induced reduction reactions that decrease oxygen content of the catalyst during the cracking process. Notably, despite these morphological changes, the global structure of the catalyst remained intact, demonstrating good thermal stability of the steel fiber catalyst.

Energy dispersive X-ray spectroscopy (EDX) analysis was conducted to characterize the elemental composition evolution of the fresh and spent catalysts. The fresh catalyst contained 85.3 wt% Fe, 5.2 wt% Mn, 5.8 wt% O, and 3.8 wt% C, with metallic components demonstrating homogeneous distributions. Nitrogen signals were found in the spent samples, consistent with the XRD analysis. Notably, the relative nitrogen content exhibited a temperature-dependent depletion profile, decreasing from 11 wt% to 2 wt% as

cracking temperature increased from 450 to 650 ℃. Concurrently, oxygen content displayed a gradually decrease trend, attributable to the in situ reduction process by on-site produced hydrogen.

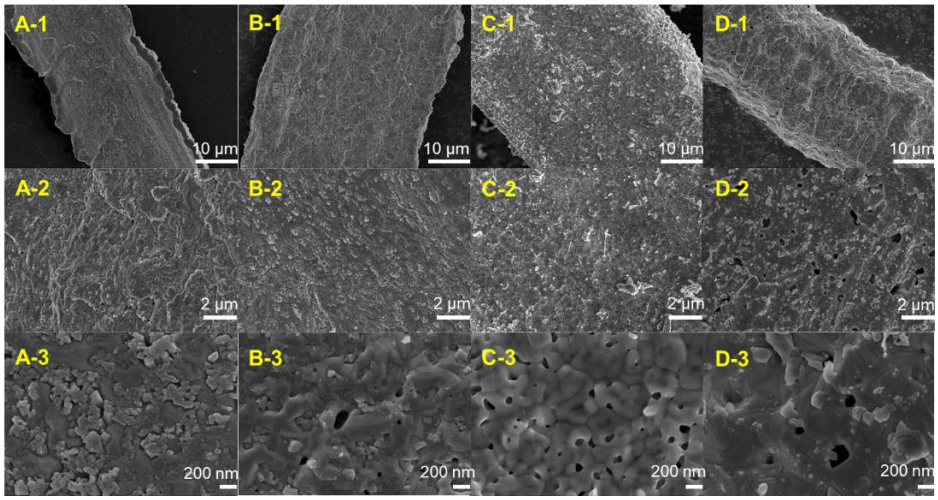

Fig. 6. Microstructures of (A) Fresh catalyst; (B) Spent catalyst at 450 ºC; (C) Spent catalyst at 550 ºC; (D) Spent catalyst at 650 ºC

Temperature-programmed characterization of the catalyst

To characterize the surface properties of the iron-based catalyst, temperature-programmed desorption (TPD) of CO_2, N_2, NH_3, and H_2, temperature-programmed reduction (H_2-TPR), and temperature-programmed oxidation (TPO) up to 900 ℃ were conducted. As shown in Fig. 7, the TPD profiles reveal distinct surface characteristics: CO_2-TPD (Fig. 7A) and NH_3-TPD (Fig. 7D) respectively identify basic and acidic sites through their characteristic desorption peaks at 625°C and 632.2°C.

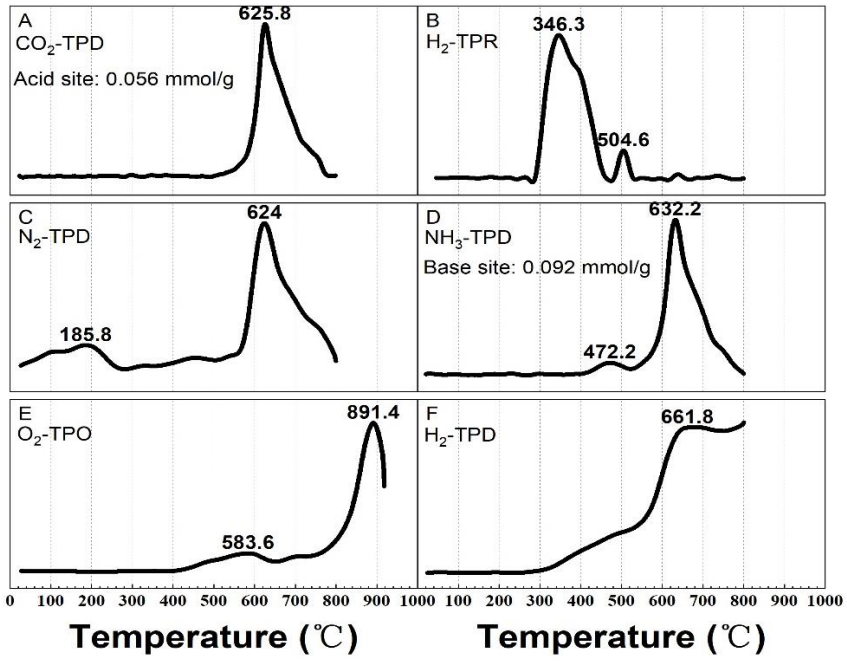

Fig. 7. Temperature-programmed characterizations of the fresh steel fiber catalyst

From the peak shift, it demonstrated a predominance of acidic sites on the catalyst surface over basic sites, indicating an acidic surface environment. The H_2-TPR profile in Fig. 7B displayed a two-stage process at 346 and 504 ℃, corresponding to the sequential reduction of surface iron and the bulk iron components. Nitrogen and hydrogen adsorption properties, as shown by N_2-TPD (Fig. 7C) and H_2-TPD (Fig. 7F), demonstrated excellent physisorption capacities toward both nitrogen and hydrogen. However, the high hydrogen desorption temperature (>400 ^{o}C) implies potential limitations in hydrogen recombination efficiency during ammonia decomposition processes. TPO analysis (Fig. 7E) reveals oxidative stability of the catalysts. Two TPO peaks are found in the profile: the smaller peak around 583 ℃ corresponds to the deep oxidation of ferric oxide (mainly FeO identified from XRD analysis), while a prominent peak at 891.4 ℃ attributed to carbonaceous species combustion.

XPS analysis of the catalyst

The Fe2p XPS spectra of the fresh and spent catalysts are presented in Fig. 8. The spectra can be successfully fitted into two main peaks and one satellite peak in the $2p_{3/2}$ region, with the $2p_{1/2}$ region exhibiting a repeated pattern at almost one-third intensity. The fresh catalyst sample comprised two iron oxidation states, Fe^{2+} and Fe^{3+}, with a high Fe^{2+}/Fe^{3+} ratio exceeding seven. Two distinct satellite peaks persisted across all spectra, maintaining consistent intensity throughout the reaction process, indicating minimal structural modification. In the fresh catalyst, Fe^{2+} was characterized by a binding energy at 710 eV accompanied by a satellite peak at 712.2 eV, while Fe^{3+} appears at 722.9 eV with a satellite at 724.8 eV. The high Fe^{2+} content aligns well from XRD analysis.

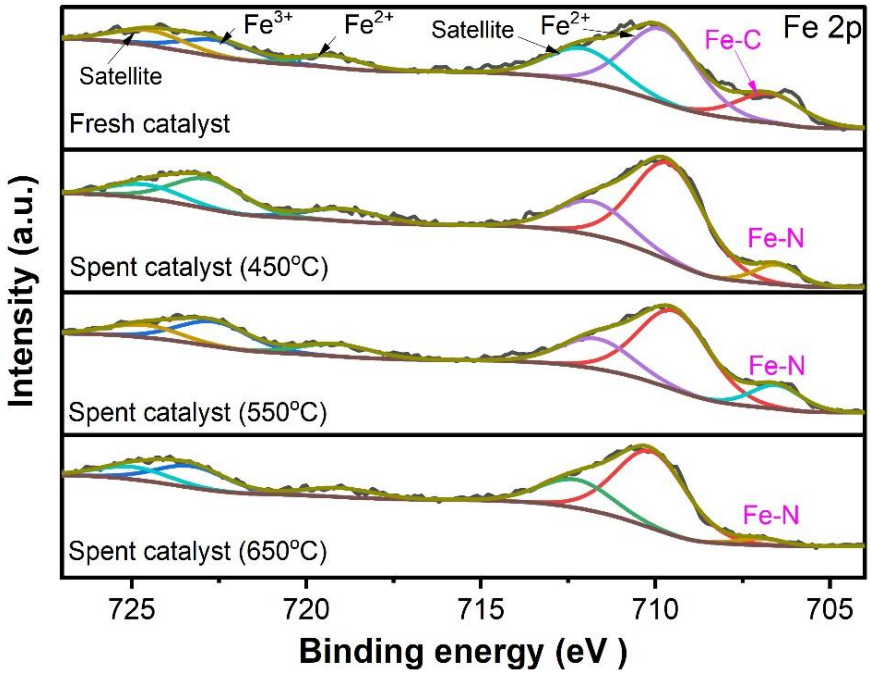

Fig. 8. The Fe2p XPS spectra of the fresh and spent steel fiber catalyst

After reaction, Fe-C in the binding energy peak at 706.8 eV transforms to the Fe-N bond at lower binding energy. However, the relative Fe-N content shows an inverse relationship with cracking temperature, suggesting enhanced nitrogen desorption at

elevated thermal conditions. A downshift in the binding energy of the Fe-N bond implies a reduction in the Fe oxidation state during the catalytic process. This electronic state modification potentially correlates with the catalyst's evolving surface chemistry, possibly influencing its catalytic performance through altered electron transfer capabilities.

DISCUSSION

The catalytic mechanism of ammonia thermal decomposition follows the opposite pathways of ammonia synthesis (Wang *et al.* 2019). The acidic surface-active sites of Fe-based fiber (TPD analysis) would be profitable for the chemisorption of the basic ammonia gas, which is the first step of the reaction. The subsequent dehydrogenation process promotes the reduction of iron oxides at temperature around 346 ℃, thereby generating additional vacant active sites for catalytic cycles. Surface recombination of hydrogen and nitrogen atoms on these sites ultimately yields gaseous H_2 and N_2 products. The overall reaction rate of the ammonia cracking is governed by the rate-limiting steps (Takahashi and Fujitani 2016), which exhibit significant dependence on catalyst composition and the active sites (Nakamura and Fujitani 2016). For noble metals (Ru, Rh, Ir, Pt, and Pd), the cleavage of N-H bonds is considered a limiting step, whereas nitrogen desorption dominates the kinetic barrier for non-noble metals (Ao *et al* 2023; Su *et al.* 2023; Skubic *et al* 2024). H_2-TPD and N_2-TPD profiles demonstrated markedly lower hydrogen desorption intensity compared with nitrogen for steel fiber catalyst, indicating it is easier to form Fe-N bonds. XPS analyses further corroborated this finding through detection of the extremely high binding energy of Fe-N (~711.3 eV), demonstrating significant energy requirements for nitrogen desorption. This interpretation is supported by XRD analysis of spent catalysts, where a higher temperature correlate with less nitrogen, which is consistent with high binding energy of Fe-N.

From the characterizations, about 5 wt% Mn was present in the steel fiber. While isolated manganese nitrides/carbides exhibit negligible activity in ammonia decomposition (Yu *et al.* 2016), synergistic effects emerge when MnN was combined with amides of alkali metals (Li, Na, and K) *via* mechanochemical processing (Guo *et al.* 2015; Yu a *et al.* 2016; Skubic *et al*. 2024). Furthermore, MnO_2 has been documented as a good support and effective promoter in ammonia decomposition catalysts (Okura *et al.* 2018). In the current catalyst system, Mn likely serves dual functions: stabilizing the fiber framework through solid-solution strengthening while potentially modulating electronic properties of the active sites to enhance ammonia cracking efficiency.

CONCLUSIONS

The steel fiber catalyst displayed exceptional activity and remarkable cyclic stability in ammonia conversion to hydrogen. The catalyst achieved notable NH_3 conversion efficiencies exceeding 63% at 600 ℃ and reaching complete conversion at 700 ℃ under 1800 mL/g/h ammonia gas space velocity. Importantly, the catalyst maintained stable performance throughout an 18-hour continuous operation across a broad temperature range (450 to 700 °C) at the same space velocity, with no detectable activity degradation observed during secondary cycling tests. Structural characterization revealed the catalyst possessed a non-porous fibrous structure containing over 80 wt% Fe atoms. XRD and XPS

analysis identified Fe_4N as the predominant active phase, which exhibited good ammonia cracking capability. Temperature-programmed desorption studies further demonstrated that elevated temperatures facilitate the nitrogen desorption and recombination on surface sites. This study establishes wool-structured iron-based catalysts as promising candidates for ammonia decomposition applications, providing fundamental insights into their structure-activity relationship. The findings hold particular significance for developing efficient catalytic systems in hydrogen energy storage and utilization technologies.

ACKNOWLEDGMENTS

This research was supported by the Natural Science Foundation of Jiangsu Province of China (BK20200892).

REFERENCES CITED

Adamou, P., Bellomi, S., Hafeez, S., Harkou, E., Al-Salem, S. M., Villa, A., and Constantinou, A. (2023). "Recent progress for hydrogen production from ammonia and hydrous hydrazine decomposition: A review on heterogeneous catalysts," *Catalysis Today* 423, article 114022. DOI: 10.1016/j.cattod.2023.01.029

Ahmed, S., Yoon,W., Jo, H., Irshad, M., Khan, M. K., and Kim, J. (2024). "Structure-activity relationship and deactivation behavior of iron oxide during CO_2 hydrogenation," *Chemical Engineering Journal* 499, article 156104. DOI: 10.1016/j.cej.2024.156104

Al-Shafei, E. N., Albahar, M. Z., Albashrayi, R., Aljishi, M., Alasseel, A., Tanimu, G., and Aitani, A. (2023). "The effect of acidic-basic structural modification of nickel-based catalyst for ammonia decomposition for hydrogen generation," *Molecular Catalysis* 550, article 113581. DOI: 10.1016/j.mcat.2023.113581

Andriani, D., and Bicer, Y. (2023). "A review of hydrogen production from onboard ammonia decomposition: Maritime applications of concentrated solar energy and boil-off gas recovery," *Fuel* 352, article 128900. DOI: 10.1016/j.fuel.2023.128900

Ao, R., Lu, R. H., Leng, G. H., Zhu, Y. R., Yan, F. W., and Yu, Q. H. (2023). "A review on numerical simulation of hydrogen production from ammonia decomposition," *Energies* 16(2), article 921. DOI: 10.3390/en16020921

Arabczyk, W., and Zamlynny, J. (1999). "Study of the ammonia decomposition over iron catalysts," *Catalysis Letters* 60, 167-171. DOI: 10.1023/A:1019007024041

Bao, Z. X., Li, D. K., Wu, Y. F., Jin, L. J., and Hu, H. Q. (2024). "Efficient Ni/Y_2O_3 catalyst prepared by sol-gel self-combustion method for ammonia decomposition to hydrogen," *International Journal of Hydrogen Energy* 53, 848-858. DOI: 10.1016/j.ijhydene.2023.11.293

Bell, T. E., and Torrente-Murciano, L. (2016). "H_2 Production *via* ammonia decomposition using non-noble metal catalysts: A review," *Topics in Catalysis* 59, 1438-1457. DOI: 10.1007/s11244-016-0653-4

Borisov, V. A., Sidorchik, I. A., Temerev, V. L., Simunin, M. M., Leont'eva, N. N., Muromtsev, I. V., Mikhlin, Y. L., Voronin, A. S., Fedorova, Z. A., Snytnikov, P. V., *et al.* (2023). "Ru-Ba/ANF catalysts for ammonia decomposition: Support

carbonization influence," *International Journal of Hydrogen Energy* 48(59), 22453-22461. DOI: 10.1016/j.ijhydene.2023.03.182

Chang, F., Guo, J. P., Wu, G. T., Wang, P. K., Yu, P., and Chen, P. (2017). "Influence of alkali metal amides on the catalytic activity of manganese nitride for ammonia decomposition," *Catalysis Today* 286, 141-146. DOI: 10.1016/j.cattod.2016.09.010

Chen, C. Q., Fan, X., Fan, S., Zhou, C., Lin, L., Luo, Y., Au, C. K., Cai, G. H., Wang, X. Y., and Jiang, L. L. (2023). "Hydrogen production from ammonia decomposition over Ni/CeO_2 catalyst: Effect of CeO_2 morphology," *Journal of Rare Earths* 41(7), 1014-1021. DOI: 10.1016/j.jre.2022.05.001

Devkota, S., Cha, J. Y., Shin, B. J., Mun, J. H., Yoon, H. C., Mazari, S. A., and Moon, J. H. (2024). "Techno-economic and environmental assessment of hydrogen production through ammonia decomposition," *Applied Energy* 358, article 122605. DOI: 10.1016/j.apenergy.2023.122605

Duan, X. Z., Qian, G., Zhou, X. G., Sui, Z. J., Chen, D., and Yuan, W. K. (2011). "Tuning the size and shape of Fe nanoparticles on carbon nanofibers for catalytic ammonia decomposition," *Applied Catalysis B-Environmental* 101(3-4), 189-196. DOI: 10.1016/j.apcatb.2010.09.017

Fang, H., Wu, S., Ayvali, T., Zheng, J., Fellowes, J., Ho, P. L., Leung, K. C., Large, A., Held, G., Kato, R., *et al.* (2023). "Dispersed surface Ru ensembles on MgO(111) for catalytic ammonia decomposition," *Nature Communications* 14(1), article 647. DOI: 10.1038/s41467-023-36339-w

Fedorova, V. A., Borisov, V. A., Pakharukova, V. P., Gerasimov, E. Y., Belyaev, V. D., Gulyaeva, T. I., Shlyapin, D. A., and Snytnikov, P.V. (2023). "Layered double hydroxide-derived Ni-Mg-Al catalysts for ammonia decomposition process: Synthesis and characterization," *Catalysts* 13(4), article 678. DOI: 10.3390/catal13040678

Ganley, J. C., Thomas, F. S., Seebauer, E. G., and Masel, R. I. (2004). "A priori catalytic activity correlations: The difficult case of hydrogen production from ammonia," *Catalysis Letters* 96, 117-122. DOI: 10.1023/B: CATL.0000030108.50691.d4

Guo, J. P., Chang, F., Wang, P. K., Hu, D. Q., Yu, P., Wu, G. T., Xiong, Z. T., and Chen, P. (2015). "Highly active MnN-LiNH composite catalyst for producing CO-free hydrogen," *ACS Catalysis* 5(5), 2708-2713. DOI: 10.1021/acscatal.5b00278

He, H., Jiang, H. J., Yang, F. Y., Liu, J., Zhang, W. X., Jin, M., and Li, Z. F. (2023). "Bimetallic Ni_xCo_{10-x}/CeO_2 as highly active catalysts to enhance mid-temperature ammonia decomposition: Kinetics and synergies," *International Journal of Hydrogen Energy* 48(13), 5030-5041. DOI: 10.1016/j.ijhydene.2022.10.255

Hu, Z. P., Chen, L., Chen, C., and Yuan, Z. Y. (2018). "Fe/ZSM-5 catalysts for ammonia decomposition to CO-free hydrogen: Effect of SiO/AlO ratio," *Molecular Catalysis* 455, 14-22. DOI: 10.1016/j.mcat.2018.05.027

Hou, C. Z., Xue, L., Li, J. Z., Ma, W. S., Wang, J. C., Dai, Y. A., Chen, C., and Dang, J. (2024). "Unlocking the potential of lattice oxygen evolution in stainless steel to achieve efficient OER catalytic performance," *Acta Materialia* 277, article120176. DOI: 10.1016/j.actamat.2024.120176

Ji, Q. H., Yu, X. J., Chen, L., Yarley, O. P. N., Zhou, C. S. (2021). "Facile preparation of sugarcane bagasse-derived carbon supported MoS_2 nanosheets for hydrogen evolution reaction," *Industrial Crops and Products* 172, article 114064. DOI: 10.1016/j.indcrop.2021.114064

Ji, Q. H., Zhou, C. S., Li, Z. Q., Boateng, I. D., Liu, X. M. (2023). "Is nanocellulose a good substitute for non-renewable raw materials? A comprehensive review of the state of the art, preparations, and industrial applications," *Industrial Crops and Product* 202, article 117093. DOI: 10.1016/j.indcrop.2023.117093

Ju, X. H., Liu, L., Zhang, T., He, T., Xu, Y. H., and Chen, P. (2024). "Ru nanoparticles on K doped γ-alumina with abundant surface superbasic sites for ammonia decomposition," *Catalysis Letters* 154(2), 473-486. DOI: 10.1007/s10562-023-04317-y

Kim, H. B., and Park, E. D. (2023). "Ammonia decomposition over Ru catalysts supported on alumina with different crystalline phases," *Catalysis Today* 411, article 113817. DOI: 10.1016/j.cattod.2022.06.032

Lee, J. E., Lee, J., Jeong, H., Park, Y. K., and Kim, B. S. (2023). "Catalytic ammonia decomposition to produce hydrogen: A mini-review," *Chemical Engineering Journal* 475, article 146108. DOI: 10.1016/j.cej.2023.146108

Li, L., Meng, Q., Ji, W. J., Shao, J. L., Xu, Q., and Yan, J. L. (2017). "Embedded iron nanoparticles by graphitized carbon as highly active yet stable catalyst for ammonia decomposition," *Molecular Catalysis* 442, 147-153. DOI: 10.1016/j.mcat.2017.09.013

Lucentini, I., Garcia, X., Vendrell, X., and Llorca, J. (2021). "Review of the decomposition of ammonia to generate hydrogen," *Industrial & Engineering Chemistry Research* 60(51), 18560-18611. DOI: 10.1021/ acs.iecr.1c00843

Ma, M., Shao, W. Q., Chu, Q. D., Tao, W. T., Chen, S., Shi, Y. Q., He, H. W., Zhu, Y. L., and Wang, X. (2024). "Structural design of asymmetric gradient alternating multilayered CNF/MXene/FeCo@rGO composite film for efficient and enhanced absorbing electromagnetic interference shielding," *Journal of Materials Chemistry A* 12(3), 1617-1628. DOI: 10.1039/D3TA06467K

Man, Y., Xu, T., Adhikari, B., Zhou, C., Wang, Y., Wang, B. (2021). "Iron supplementation and iron-fortified foods: A review," *Critical Reviews in Food Science and Nutrition* 62(16), 4504-4525. DOI: 10.1080/10408398.2021.1876623

Naseem, Z., Iqbal, J., Zahid, M., Shaheen, A., Hussain, S., and Yaseen, W., (2020). "Use of hydrogen-bonded supramolecular eutectic solvents for eco-friendly extraction of bioactive molecules from using Box-Behnken design," *Journal of Food Measurement and Characterization* 15, 1487-1498. DOI: 10.1007/s11694-020-00744-2

Nakamura, I., and Fujitani, T. (2016). "Role of metal oxide supports in NH_3 decomposition over Ni catalysts," *Applied Catalysis A: General* 524, 45-49. DOI: 10.1016/j.apcata.2016.05.020

Nuss, P., and Eckelman, M. J. (2014). "Life cycle assessment of metals: A scientific synthesis," *Plos One* 9(7), article e101298. DOI: 10.1371/journal.pone.0101298

Okura, K., Miyazaki, K., Muroyama, H., Matsui, T., and Eguchi, K. (2018). "Ammonia decomposition over Ni catalysts supported on perovskite-type oxides for the on-site generation of hydrogen," *RSC Advances* 8(56), 32102-32110. DOI: 10.1039/C8RA06100A

Ren, M. N., Kong, F. G., Zhou, C. S., Fakayode, O. A., Liang, J. K., Li, H. X., Zhou, M., Fan, X. Y. (2023). "Green, one-pot biomass hierarchical utilization strategy for lignin-containing cellulose nanofibrils and fractionated lignin preparation," *Industrial Crops and Products* 203, article 117193. DOI: 10.1016/j.indcrop.2023.117193

Skubic, L., Gyergyek, S., Hus, M., and Likozar, B. (2024). "A review of multiscale modelling approaches for understanding catalytic ammonia synthesis and decomposition," *Journal of Catalysis* 429, article 115217. DOI: 10.1016/j.jcat.2023.115217

Su, T. X., Guan, B., Zhou, J. F., Zheng, C. Z., Guo, J. F., Chen, J. Y., Zhang, Y.Y., Yuan, Y. H., Xie, W. K., Zhou, N. X., *et al.* (2023). "Review on Ru-based and Ni-based catalysts for ammonia decomposition: Research status, reaction mechanism, and perspectives," *Energy & Fuels* 37(12), 8099-8127. DOI: 10.1021/acs.energyfuels.3c00804

Takahashi, A., and Fujitani, T. (2016). "Kinetic analysis of decomposition of ammonia over nickel and ruthenium catalysts," *Journal of Chemical Engineering of Japan* 49(1), 22-28. DOI: 10.1252/jcej.14we431

Wang, Y. X., Kunz, M. R., Fang, Z. T., Yablonsky, G., and Fushimi, R. (2019). "Accumulation dynamics as a new tool for catalyst discrimination: An example from ammonia decomposition," *Industrial & Engineering Chemistry Research* 58(24), 10238-10248. DOI: 10.1021/acs.iecr.9b01470

Xie, P. F., Yao, Y. G., Huang, Z. N., Liu, Z. Y., Zhang, J. L., Li, T. Y., Wang, G. F., Shahbazian-Yassar, R., Hu, L. B., and Wang, C. (2019). "Highly efficient decomposition of ammonia using high-entropy alloy catalysts," *Nature Communications* 10(1), article 4011. DOI: 10.1038/s41467-019-11848-9

Xun, Y. R., He, X. X., Yan, H., Gao, Z. W., Jin, Z., and Jia, C. J. (2017). "Fe- and Co-doped lanthanum oxides catalysts for ammonia decomposition: Structure and catalytic performances," *Journal of Rare Earths* 35(1), 15-23. DOI: 10.1016/S1002-0721(16)60167-9

Yu, P., Guo, J. P., Liu, L., Wang, P. K., Wu, G. T., Chang, F., and Chen, P. (2016). "Ammonia decomposition with manganese nitride-calcium imide composites as efficient catalysts," *ChemSusChem* 9(4), 364-369. DOI: 10.1002/cssc.201501498

Yu, C. J., Zhang, D. B., Liu, Z. G., Wu, D. S., Zhong, Y. L., Wu, J. Z. (2025). "Study on nitrogen pores, microstructure, and mechanical properties of nickel-free high-nitrogen stainless steel fabricated via LDED regulated by heat input, " *Virtual and Physical Prototyping* 20(1), article e2445711. DOI: 10.1080/17452759.2024.2445711

Zhai, X. D., Wang, X. Y., Zhang, J. J., Yang, Z. K., Sun, Y., Li, Z. H., Huang, X. W., Holmes, M., Gong, Y. Y., Povey, M., Shi, J. Y, Zou, X. B. (2020). "Extruded low density polyethylene-curcumin film: A hydrophobic ammonia sensor for intelligent food packaging," *Food Packaging and Shelf Life* 26, article 100595. DOI: 10.1016/j.fpsl.2020.100595

Zhang, J., Comotti, M., Schüth, F., Schlögl, R., and Su, D. S. (2007). "Commercial Fe- or Co containing carbon nanotubes as catalysts for NH_3 decomposition," *Chemical Communications* 19, 1916-1918. DOI: 10.1039/B700969K

Zhang, L., Zhang, B., Yang, Z. Q., Yan, Y. F. (2014). "Pyrolysis behavior of biomass with different Ca-based additives," *RSC Advances* 4, 29145-29155. DOI: 10.1039/c4ra04865b

Zhang, T., Zhao, B. C., Chen, Q. Y., Peng, X. M., Yang, D. Y., and Qiu, F. X. (2019). "Layered double hydroxide functionalized biomass carbon fiber for highly efficient and recyclable fluoride adsorption," *Applied Biological Chemistry* 62, article 12. DOI: 10.1186/s13765-019-0410-z

Zhang, H., Alhamed, Y. A., Kojima, Y., Al-Zahrani, A. A., and Petrov, L. A. (2023). "Cobalt supported on carbon nanotubes. An efficient catalyst for ammonia decomposition," *Comptes Rendus de l'Académie Bulgare des Sciences* 66(4), 519-524. DOI: 10.7546/CR-2013-66-4-13101331-7

Article submitted: September 3m 2024; Peer review completed: February 13, 2025; Revised version received: March 1, 2025; Accepted: March 4, 2025; Published: April 24, 2025.
DOI: 10.15376/biores.20.2.4416-4431